# Preliminary design of control rods in the Single-fluid Double-zone Thorium Molten Salt Reactor (SD-TMSR): Part 1

O. Ashraf[a,b,*], Andrei Rykhlevskii[c], G. V. Tikhomirov[a], Kathryn D. Huff[c]

[a] *Dept. of Theoretical and Experimental Physics of Nuclear Reactors, Institute of Nuclear Physics and Engineering, National Research Nuclear University MEPhI, 31, Kashirskoe Shosse, Moscow, 115409, Russian Federation*
[b] *Physics Department, Faculty of Education, Ain Shams University, Cairo, Egypt, 11341*
[c] *Dept. of Nuclear, Plasma, and Radiological Engineering, University of Illinois at Urbana-Champaign, Urbana, IL 61801, United States*

**Abstract**

The current work is focused on.....

*Keywords:* MSR, thorium fuel cycle, control rod, safety, online reprocessing, Monte carlo code

## 1. Introduction

The Generation IV International Forum (GIF) [1] determined six innovative reactor systems: the Very High-Temperature Reactor (VHTR), the Molten Salt Reactor (MSR), the Supercritical Water-Cooled Reactor (SWCR), the Gas-cooled Fast Reactor (GFR), the Sodium-cooled Fast Reactor (SFR), and the Lead-cooled Fast Reactor (LFR). The MSR is the only liquid-fueled reactor among these reactors. Major nuclear centers pursue MSRs with renewed interest [2, 3, 4, 5, 6]. The MSR is a promising technology because of its dynamics, especially for thorium fuel utilization. However, this technology has challenges in safety, online reprocessing, and fuel handling. Safety is one of the technological goals of the MSR systems that require further research and investigation. The unique characteristics of the MSRs (liquid fuel, flux level, neutron economy,

*Corresponding Author
*Email address:* osama.ashraf@edu.asu.edu.eg oabdelaziz@mephi.ru (O. Ashraf)

etc.) strongly affect its control system design. The MSRs have a negative temperature coefficient of reactivity. Doppler effect and thermal expansion of the fuel reduce core reactivity when the core heats up. However, graphite thermal expansion positively affect the core reactivity [7]. The graphite expansion is not a dominating factor, thus core reactivity will decrease automatically when the core heats up [8]. The MSR designs have a drain tank to collect the liquid fuel in an emergency case. A freeze plug, which located under the core, melts when the temperature reaches a critical point. Then the fuel moves to the drain tank to shut down the reactor [9]

Safety aspects in the MSRs can be listed as follows [9, 10]:

1. The negative coefficient of reactivity - high core temperature will reduce reactivity.
2. The fuel feed rate - decreasing the refueling rate slows down and eventually stops the nuclear chain reaction.
3. The drain tanks, which have subcritical geometry and passively cooled.
4. The control rods compensate the excess reactivity, temperature regulation, and/or shut down the reactor.
5. The continuous removing of fission products and radioactive gasses minimize the chance of radiation exposure.
6. The reactor system chamber.
7. The outer containment vessel.

At the Beginning of Life (BOL), we must load the MSR with larger amount of fuel than that required to achieve criticality (necessary for long term core operation). This leads to excess reactivity at the BOL [11]. Additionally, during burnup, the online reprocessing and refueling leads to change the reactivity of the MSRs [3]. The most common procedure for reactor control is to insert or withdraw control rods with large neutron absorption cross section (e.g. boron and cadmium) [11]. The control rods introduce an amount of negative reactivity into the core. This negative reactivity helps to compensate the excess reactivity and adjust the power level of the core or even shut down the reactor in an emergency situation [12]. Therefore, we should estimate the reactivity worth of the control rods [13, 14, 15, 16]. The reactivity worth of control rods correlates with the interference (shadowing effects) between control rod clusters. [17, 18]. The control rod worth and its efficiency to absorb excess positive reactivity is a subject of major interest since it directly affects reactor safety [19, 20, 18, 21, 22, 13].

Boron carbide ($B_4C$) is used in control rods [23, 24, 25]. However, we may need to enrich the effective boron isotope ($^{10}B$) to reach the necessary absorptivity. Notably, the spatial self-shielding effect correlates with $^{10}B$ concentration. For example, $B_4C$ enriched to 90% contains $^{10}B$ 4.5 times larger than in natural $B_4C$, however, its absorption ability is about 2.3 times compared with natural $B_4C$. Additionally, issues related to helium gas release, swelling, melting risk, and high loss of the reactivity worth limit the $B_4C$ lifespan [26].

Guo (2019), Gosset (2017), and Rudy (2011) summarized the properties of the potential alternative absorbers in Generation-IV reactors such as hafnium-based materials and rare earth element oxides. These absorbers have high thermal conductivity, good resistance to neutron irradiation, and release no gas [26, 27, 28].

The Single-fluid Double-zone Thorium-based Molten Salt Reactor (SD-TMSR) with a thermal power of 2250 $MW_{th}$ [3, 8] is a graphite-moderated molten salt reactor. Recent studies on MSRs show that the excess reactivity at the beginning of the operation is quite large for many fueling scenarios [3, 29, 4, 30, 31]. Adjusting fertile and fissile feed rates helps to control the reactivity of the SD-TMSR [3]. However, we should introduce a reliable safety system beside the online feed system to control the excess reactivity. Therefore, the main objective of our study is to introduce a new safety system based on control rods in the SD-TMSR to control the reactivity during normal operation. Five different absorber materials are applied to study the main neutronics and safety parameters in the SD-TMSR. We focus on the control rod design, absorption ability, integral and differential control rod worths, shutdown margin of absorber materials, and shadowing effects at steady state calculation.

Čerba *et al.* (2017) designed a reactivity control system in the GFR. They utilized the MCNP5 [33] and KENO6 codes [34] to calculate the reactivity worth and analyze the performance of this control system [18]. Since no final geometry design of the control rods system is available for the SD-TMSR, Čerba's methodology [18] helped us as a starting point of this analysis.

All calculations presented in this work are performed using Monte-Carlo code SERPENT-2 version 2.1.31 [35].

This paper is organized as follows: section 2 discusses the reactor and control rod design, section 3 describes methodology and tools, section 4 focuses on the results and discussion, and section 5 highlights the conclusions.

## 2. Model description

### *2.1. Reactor design*

The Single-fluid Double-zone Thorium-based Molten Salt Reactor (SD-TMSR) design was proposed by the Chinese Academy of Sciences in 2011 [8, 36, 37, 38]. The SD-TMSR is a graphite-moderated molten salt reactor with a thermal power of 2250 $MW_{th}$. The design of the SD-TMSR is inspired by the Molten Salt Breeder Reactor (MSBR) [39] and the Thorium-based Molten Salt Reactor (TMSR) [40] after modifying the geometry to control the positive temperature coefficient in the MSBR. The SD-TMSR core geometry is described in detail by Li *et al.* and Ashraf *et al.* [8, 3]. The active zone of the SD-TMSR is a right cylinder divided into the inner zone (486 fuel tubes) and the outer zone (522 fuel tubes) to enhance breeding performance.

In this study, the fuel salt composition is 70LiF - 17.5$BeF_2$ - 12.5$(HM)F_4$ mole%, where HM is the heavy metal (i.e. $^{232}$Th and fissile materials). Three different types of initial fissile materials are considered: (1) $^{233}$U [3], (2) reactor-grade Pu [41], and (3) transuranic (TRU) elements from Light Water Reactor (LWR) LWR spent nuclear fuel (SNF) [42]. The density and volume of the fuel

Table 1: The main characteristics of the SD-TMSR [8].

| | |
|---|---|
| Thermal power, $MW_{th}$ | 2,250 |
| Fuel salt components | $LiF$-$BeF_2$-$(HM)F_4$ |
| Fuel composition, mole% | 70-17.5-12.5 |
| $^7Li$ enrichment, % | 99.995 |
| Fuel temperature, K | 900 |
| Fuel density at 900 K, g/cm$^3$ | 3.3 |
| Fuel dilatation coefficient, g/(cm$^3$.K) | $-6.7\times10^{-4}$ |
| Graphite density, g/cm$^3$ | 2.3 |
| $B_4C$ density, g/cm$^3$ | 2.52 |
| $^{10}B$ enrichment, % | 18.4 |
| Core diameter, cm | 460 |
| Core height, cm | 460 |
| Side length of the graphite hexagonal prism, cm | 7.5 |
| Inner radius, cm | 3.5 |
| Outer radius, cm | 5 |
| Ratio of molten salt and graphite in the inner zone | 0.357 |
| Ratio of molten salt and graphite in the outer zone | 1.162 |
| Fuel volume, m$^3$ | 52.9 |

salt are 3.3 g/cm$^3$ and 52.9 m$^3$, respectively. The liquid fuel salt circulates continuously through the fuel tubes that pierce the graphite hexagonal prisms. The active zone is surrounded by axial and radial graphite reflectors to minimize the neutron leakage. Finally, the SD-TMSR pressure vessel holds all reactor components and is made of a Hastelloy N alloy. The main characteristics of the SD-TMSR are summarized in Table 1.

### *2.2. Control rod design*

The reactivity of the SD-TMSR core is controlled through two systems of control assemblies:

1. The Control Safety Devices (CSD), and
2. The Shutdown Safety Devices (SSD).

The CSD system is designed for reactivity control during normal operation and the SSD system is designed for an emergency reactor shutdown. In the present work, five different absorber materials are considered based on their neutronics and safety performance:

1. $B_4C$ with boron enriched to 90% $^{10}B$ isotope,
2. hafnium diboride ($HfB_2$),
3. hafnium hydride ($HfH_{1.62}$),
4. gadolinium oxide ($Gd_2O_3$), and
5. europium oxide ($Eu_2O_3$).

Boron carbide ($B_4C$) is widely used in control rods fabrication. Enriching $B_4C$ increases the fraction of highly neutron absorber isotope (i.e. $^{10}B$) and helps to reach the necessary absorptivity. However, issues related to helium gas release through (n,$\alpha$) reactions of $^{10}B$, swelling, melting risk, and high loss of the reactivity worth limit the $B_4C$ lifespan [26]. Hafnium and rare earth elements oxides absorb neutrons through (n,$\gamma$) reactions and this limits gas emission.

The control rod is a cylinder with a radius of 0.75 cm and a height of 520 cm. The absorber material is surrounded by a 0.25-cm-thick clad made of AIM1 (15Cr-15Ni) steel alloy [43] and the rod follower is made of SiC structural material (see Figure 1). A small gap between the cladding and rod follower is considered to facilitate the control rod movement.

Since the total quantity and distribution of the SD-TMSR control assemblies are unknown, we proposed an original distribution as a starting point of this analysis. We added clusters consist of four control rods to specific graphite hexagonal prisms (elements) in the SD-TMSR core. Every four control rods (cluster) can move together as one group. Figure 2 and 3 demonstrate the plan

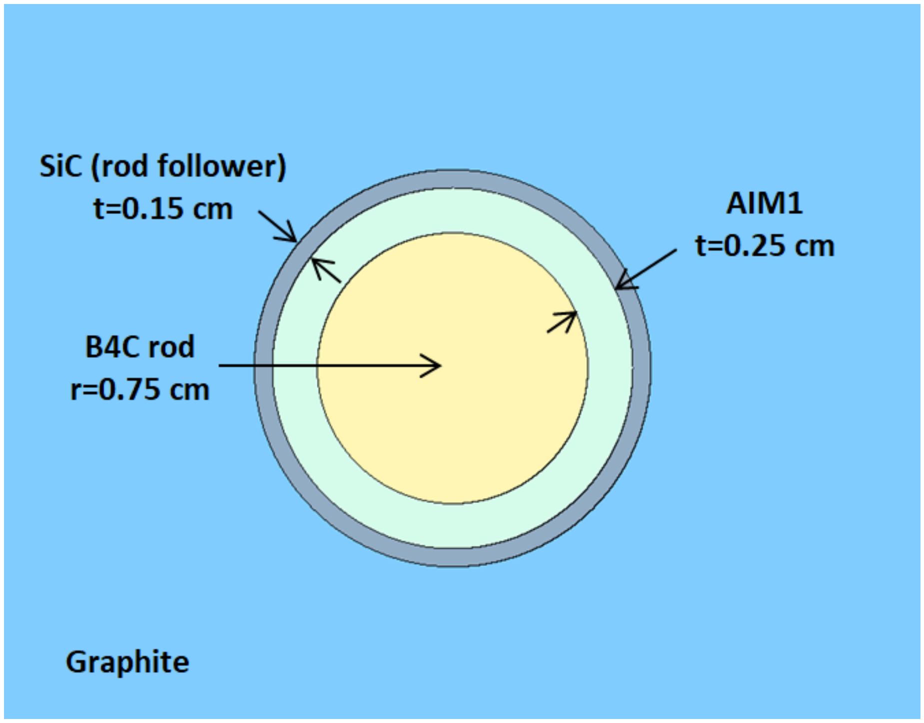


Figure 1: Cross section of the $B_4C$ control rod.

and axial view of the graphite element with the four control rods. The total numbers of graphite elements with control rods are 25: 16 CSD and 9 SSD.

Figure 4 illustrates the numbering scheme of control rods clusters in the SD-TMSR core. The CSD1-16 clusters are represented as yellow color and distributed as two rings: inner and outer ring (peripheral ring). The inner ring includes CSD from 1 to 6, while the outer ring includes CSD from 7 to 16. Red color stands for SSD1-9 clusters. We distributed the graphite elements with control rods clusters homogeneously in the inner core of the SD-TMSR, where the moderator-to-fuel ratio is high. The selected core segment in the above corner of the Figure 4 shows that both CSD and SSD clusters consist of four control rods located at the same distance from the fuel channel.

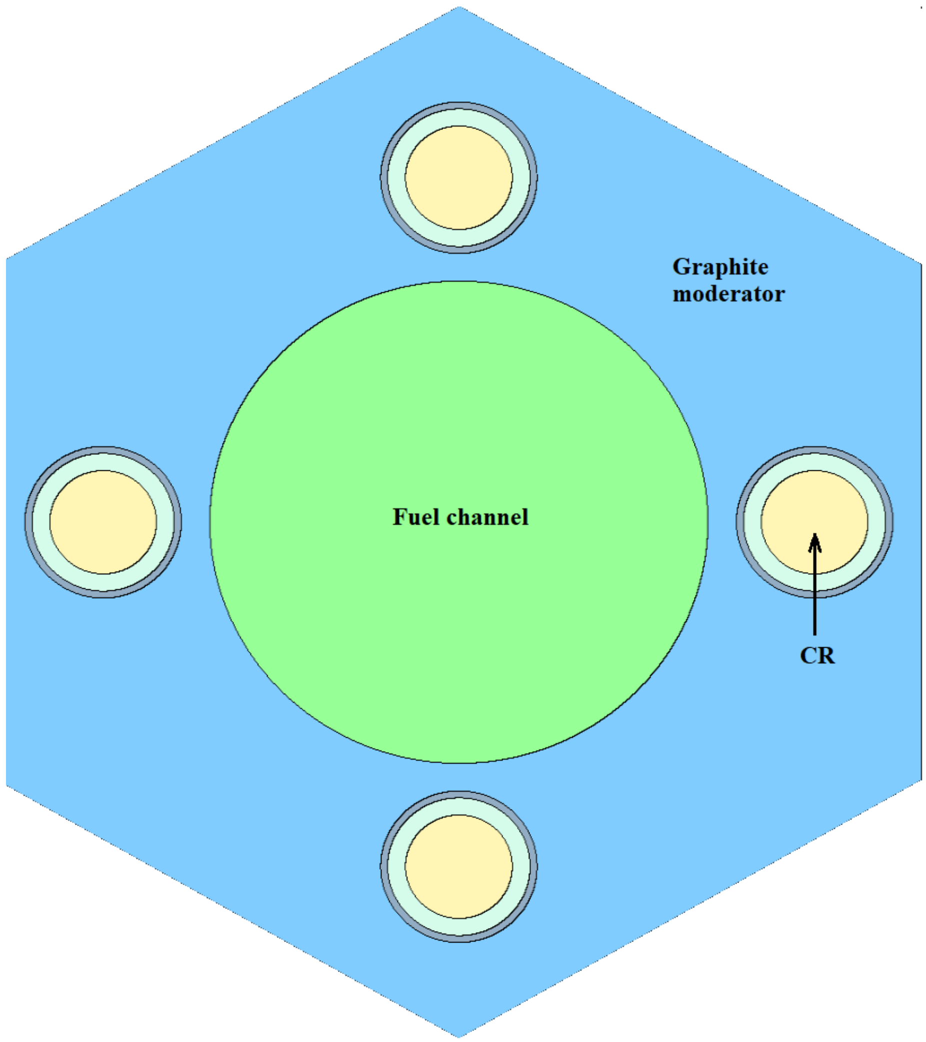


Figure 2: Graphite element with the four control rods (cluster) located at the same distance from the fuel channel.

## 3. Methodology and tools

### *3.1. Control rod design evaluation*

In this work, SERPENT-2 version 2.1.31 [35] is used to perform steady state calculations for the full-core of the Single-fluid Double-zone Thorium-based Molten Salt Reactor (SD-TMSR) with control rod design. We adopted the

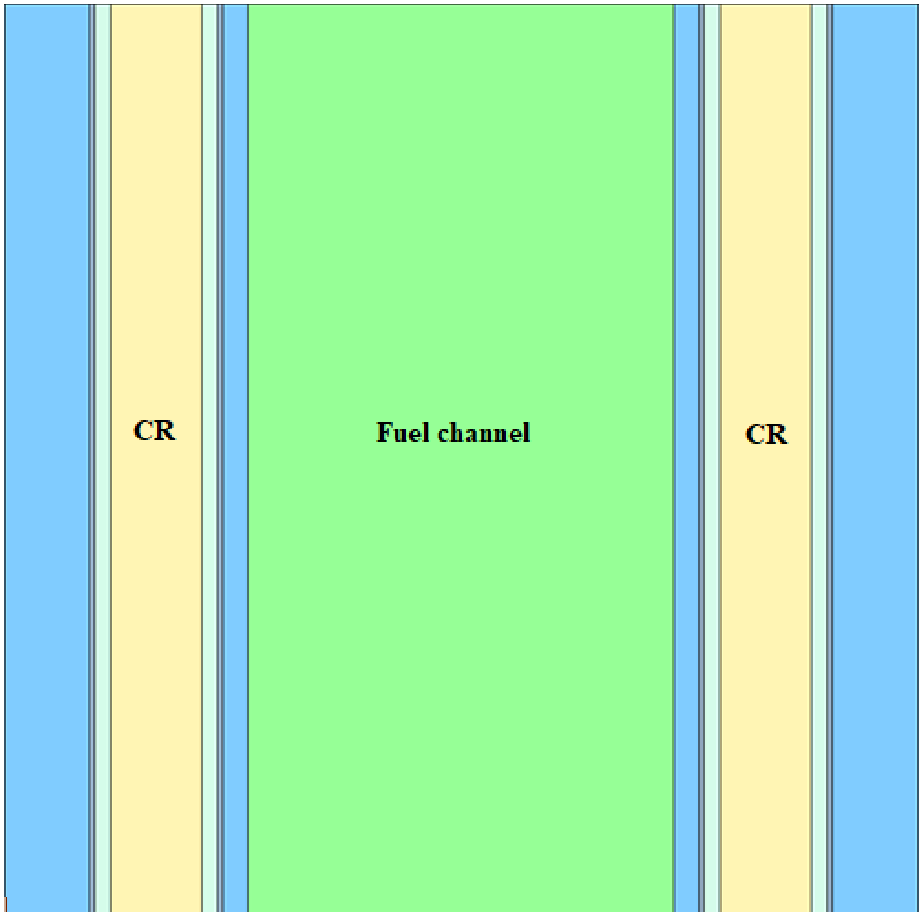


Figure 3: Axial view of graphite element with control rods.

ENDF-VII.0 cross section library for all calculations in the present work. The results demonstrate whole-core runs of $12.5 \times 10^6$ neutron histories per depletion step. The statistical error in $k_{eff}$ from SERPENT-2 output is equal to $\pm$ 25 $pcm$.

The initial calculation state of the SD-TMSR is identified by normal operation conditions (see Table 1) and fully withdrawn control rods clusters. In this case, the control rods are located above the upper plenum as shown in Figure 5. To validate the proposed control rods system we adopted the same operation conditions (as in the initial case) and changed the position of the control rod

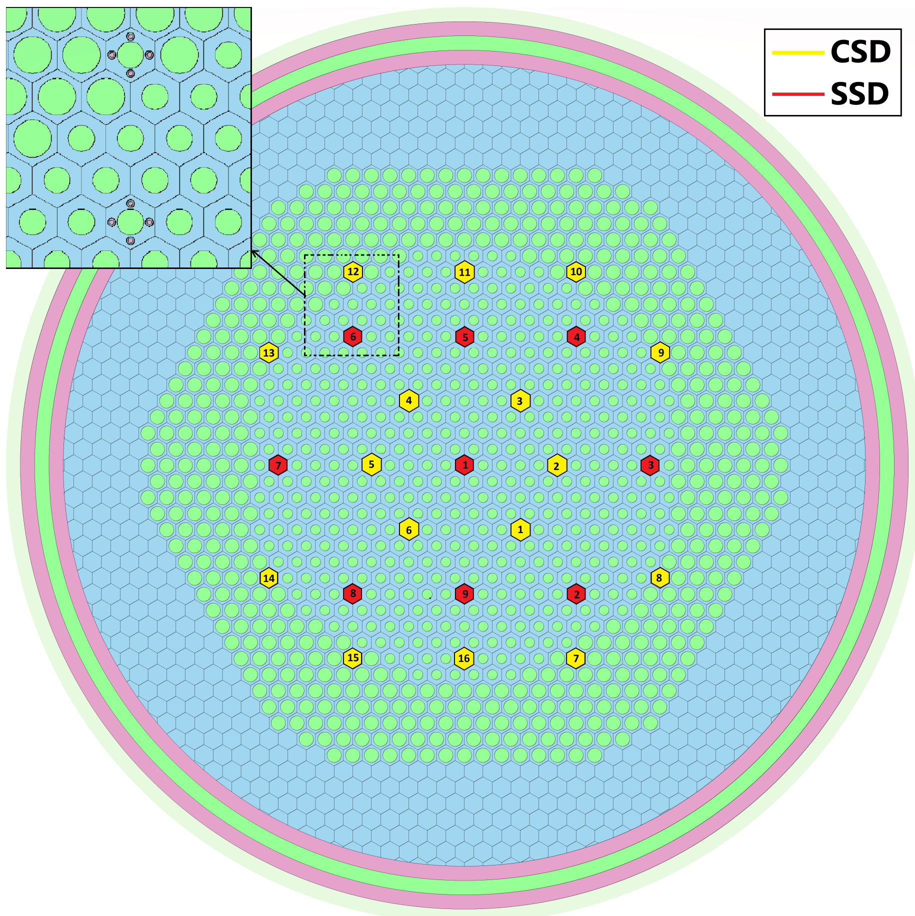


Figure 4: Distribution of the graphite elements with control rods in the SD-TMSR core.

clusters along $Z$ direction. The main calculated parameters including reactivity, control rod worth, and interference effects (shadowing effects) will describe in the following parts.

*3.1.1. Reactivity calculation*

The excess reactivity $\rho_e$ is the reactivity of the core when all control rods are withdrawn. $\rho_e$ is calculated by SERPENT-2 in \$ units based on equation 1, where $k_{eff}$ is the effective multiplication factor of the core and $\beta_{eff}$ is the effective fraction of delayed neutrons. The effective delayed neutron fraction is

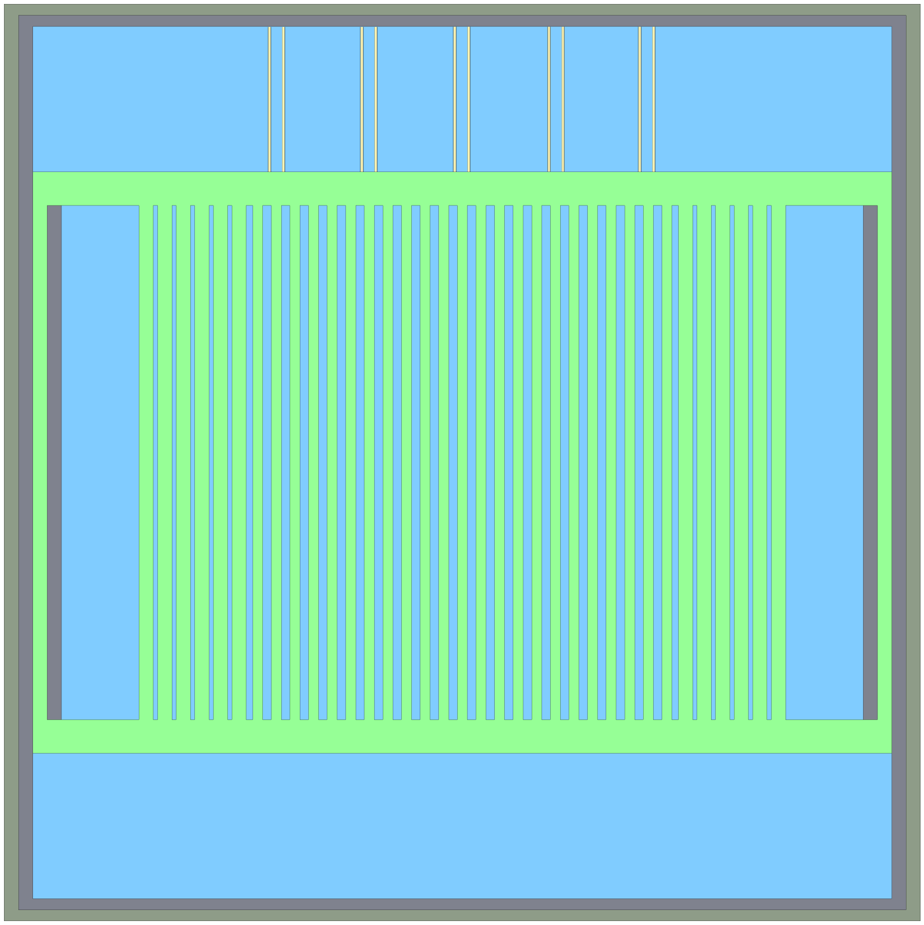

Figure 5: $XZ$ section of the full-core model of the SD-TMSR, CRs are fully withdrawn.

calculated by the adjoint-weighted time constants using perturbation technique in SERPENT-2 [44].

$$\rho_e = \frac{k_{eff} - 1}{k_{eff}\beta_{eff}}, \tag{1}$$

*3.1.2. The control rod worths (CRW)*

The control rod worth (CRW) is the amount of negative reactivity that associated with the control rod insertion. The CRW is calculated by SERPENT-2 in \$ units based on equation 2, where $\Delta\rho_{CRi}$ is the worth of i$^{th}$ CR, $\rho_e$ is the initial excess reactivity, and $\rho_{CRi}$ is the excess reactivity after i$^{th}$ CR insertion [18].

$$\Delta\rho_{CRi} = \rho_e - \rho_{CRi}, \tag{2}$$

#### 3.1.3. Shutdown Margin (SDM)

The shutdown margin (SDM) is the amount of reactivity by which a full reactor core is subcritical from a given state. The SDM is expressed in terms of reactivity and calculated by equation 3, where $\Delta\rho_{SSD}$ is the total worth of the Shutdown Safety Devices (SSD) and $\rho_e$ is the core excess reactivity.

$$SDM = \Delta\rho_{SSD} - \rho_e, \tag{3}$$

#### 3.1.4. Interference effects (shadowing effects)

Interference between control rods (CRs) or shadowing effects occurs when one (or more) control rod affects the reactivity worth of another control rod in the surroundings. Thus, anti-shadowing is observed when the combined rod worth is greater than the sum of the individual worths, however, the shadowing effect appears when the combined rod worth is less than the sum of the individual worths. The core height-to-diameter ratio (H/D) and the three-dimensional configuration of the control rods affect the degree of the interference between CRs [32].

The amplification factor (A$_{CRi}$) of i$^{th}$ control rod helps to evaluate the shadowing effects between control rod clusters. The amplification factor is calculated by equation 4 [32, 18], where $\Delta\rho_{CR(1,2,...N)}$ is the total worth of all control rods (from 1 to $N$), $\Delta\rho_{CR(1,2,...N-i)}$ is the total worth of all CRs except the investigated one i$^{th}$ and $\Delta\rho_{CRi}$ the worth of the i$^{th}$ rod.

$$A_{CRi} = \frac{\Delta\rho_{CR(1,2,...N)} - \Delta\rho_{CR(1,2,...N-i)}}{\Delta\rho_{CRi}}, \tag{4}$$

If A$_{CRi}$ is $<$1, the control rod worth is reduced due to shadowing effects, while if A$_{CRi}$ is $>$1 the control rod worth is amplified and anti-shadowing effects occur. $A_{CRi} = 1$ means no shadowing effects occur.

### 3.1.5. Integral and differential control rod worth

The integral CRW is the total reactivity change due to control rod insertion or withdrawal. However, the differential CRW is the amount of reactivity inserted per unit of withdrawal [$\$/cm$]. We change the position of CRs clusters parallel to the z-axis from top to the bottom of the core. Equation 5 is used to calculate the integral CRW [\$], where $k_i$ and $k_{i-1}$ are the effective multiplication factor after and before CR insertion to i$^{th}$ step. $\beta_i$ is the effective fraction of delayed neutrons at i$^{th}$ step. N is the number of steps.

$$\Delta\rho_i = \sum_{i=1}^{N} \frac{k_i - k_{i-1}}{k_i k_{i-1} \beta_i}, \tag{5}$$

Equation 6 is used to calculate the differential CRW [\$/cm], where $\Delta H$ is the height change of control rod [cm] before and after insertions.

$$\frac{\partial\rho_i}{\partial H} = \frac{1}{\Delta H} \frac{k_i - k_{i-1}}{k_i k_{i-1} \beta_i}, \tag{6}$$

## 4. Results and discussion

### 4.1. The excess reactivity $\rho_e$

The full-core of the Single-fluid Double-zone Thorium-based Molten Salt Reactor (SD-TMSR) is loaded by three different types of initial fissile materials: $^{233}$U, reactor-grade Pu, and transuranic (TRU) elements from LWR SNF. The excess reactivity $\rho_e$ is calculated at zero burnup (steady state calculation), when all CRs are fully withdrawn. The excess reactivities for $^{233}$U, reactor-grade Pu, and TRU are $1.65 \pm 0.04$ \$, $4.11 \pm 0.02$ \$, and $15.38 \pm 0.04$ \$, respectively. For $^{233}$U case, the maximum excess reactivity $\rho_e$ is about $4.27 \pm 0.01$ \$ during 60 effective full-power years (EFPY) of reactor operation (see Figure 6). The SD-TMSR is able to control the reactivity by adjusting the online refueling and reprocessing rates. An effective and reliable reactivity control system must be

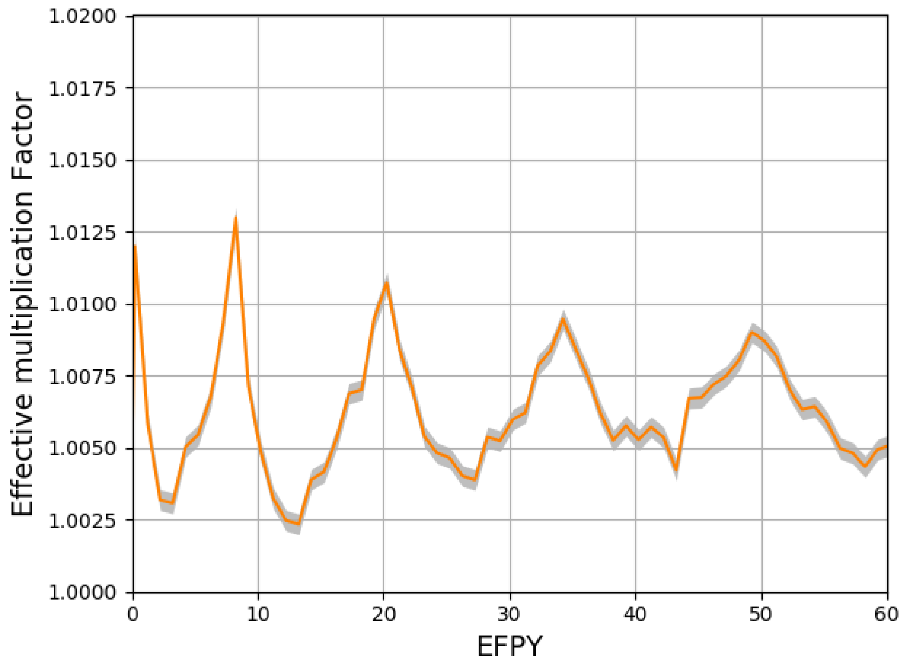


Figure 6: The change of the effective multiplication factor during 60 EFPY of reactor operation including periodic fissile material insertion (confidence interval $\pm\sigma$ is shaded) [3].

designed beside the online feed system to operate with such reactivity changes during burnup.

### *4.2. Control rod parameters*

The control rod parameters including control rod worth (CRW), interference between CR clusters, and integral and differential control rod worths are described in this part. Five different absorber materials are considered based on their neutronics and safety performance (see part 2.2). The results of the control rod worth, the amplification factor ($A_{CRi}$), and the type of interference for the five absorber materials are listed in Table 2.

#### *4.2.1. CRW*

The total worth of all control rods ranges from $33.7 \pm 0.4$ to $48.19 \pm 0.68$ \$ (Table 2). Enriched $B_4C$-90 has the largest absorption ability, while $Gd_2O_3$ has the lowest absorption compared with the other absorber materials in this study.

Table 2: The control rod worths and shadowing effects for different CR materials.

| CR clusters | $B_4C$-90 | | | $HfB_2$ | | | $HfH_{1.62}$ | | | $Gd_2O_3$ | | | $Eu_2O_3$ | | |
|---|---|---|---|---|---|---|---|---|---|---|---|---|---|---|---|
| | $\Delta\rho_{CRi}$ [$] | $A_{CRi}$ | Interference | $\Delta\rho_{CRi}$ [$] | $A_{CRi}$ | Interference | $\Delta\rho_{CRi}$ [$] | $A_{CRi}$ | Interference | $\Delta\rho_{CRi}$ [$] | $A_{CRi}$ | Interference | $\Delta\rho_{CRi}$ [$] | $A_{CRi}$ | Interference |
| ALL CRs | 48.19 ± 0.68 | | | 40.4 ± 0.41 | | | 37.96 ± 0.36 | | | 33.7 ± 0.4 | | | 42.39 ± 0.48 | | |
| CSD | 25.5 ± 0.23 | 1.24 ± 0.01 | ⋆ | 21.9 ± 0.17 | 1.1 ± 0.01 | ⋆ | 20.62 ± 0.34 | 1.1 ± 0.01 | ⋆ | 18.48 ± 0.25 | 1.17 ± 0.01 | ⋆ | 22.96 ± 0.18 | 1.2 ± 0.01 | ⋆ |
| SSD | 16.39 ± 0.11 | 1.38 ± 0.02 | ⋆ | 14.27 ± 0.21 | 1.29 ± 0.01 | ⋆ | 13.23 ± 0.18 | 1.3 ± 0.06 | ⋆ | 12 ± 0.2 | 1.26 ± 0.01 | ⋆ | 14.58 ± 0.11 | 1.3 ± 0.02 | ⋆ |
| CSD inner ring | 18.42 ± 0.05 | 1.6 ± 0.04 | ⋆ | 16.29 ± 0.29 | 1.48 ± 0.02 | ⋆ | 15.5 ± 0.17 | 1.46 ± 0.01 | ⋆ | 14.12 ± 0.07 | 1.39 ± 0.01 | ⋆ | 16.92 ± 0.13 | 1.5 ± 0.01 | ⋆ |
| CSD outer ring | 2.26 ± 0.02 | 4.21 ± 0.07 | ⋆ | 2.1 ± 0.06 | 3.11 ± 0.1 | ⋆ | 1.85 ± 0.07 | 3.24 ± 0.06 | ⋆ | 1.8 ± 0.1 | 2.54 ± 0.14 | ⋆ | 2.14 ± 0.05 | 3.2 ± 0.05 | ⋆ |
| CSD2 | 2.25 ± 0.04 | 3.69 ± 0.16 | ⋆ | 2.24 ± 0.05 | 2.42 ± 0.1 | ⋆ | 2 ± 0.1 | 2.68 ± 0.03 | ⋆ | 1.8 ± 0.1 | 2.55 ± 0.2 | ⋆ | 2.19 ± 0.12 | 2.9 ± 0.08 | ⋆ |
| CSD9 | 0.15 ± 0.04 | 10.53 ± 0.01 | ⋆⋆ | 0.1 ± 0.05 | 5.1 ± 0.05 | ⋆ | 0.05 ± 0.01 | 16.4 ± 0.1 | ⋆⋆ | 0.09 ± 0.07 | 5.55 ± 0.2 | ⋆⋆ | 0.07 ± 0.05 | 14 ± 0.1 | ⋆⋆ |
| SSD1 | 4.18 ± 0.07 | 1.59 ± 0.08 | ⋆ | 3.95 ± 0.13 | 1.3 ± 0.07 | ⋆ | 3.59 ± 0.03 | 1.49 ± 0.01 | ⋆ | 3.45 ± 0.12 | 1.4 ± 0.08 | ⋆ | 3.91 ± 0.06 | 1.4 ± 0.01 | ⋆ |
| SSD4 | 0.57 ± 0.09 | 7.84 ± 0.15 | ⋆⋆ | 0.63 ± 0.06 | 4.4 ± 0.1 | ⋆ | 1 ± 0.05 | 2.51 ± 0.16 | ⋆ | 0.6 ± 0.8 | 3.31 ± 0.27 | ⋆ | 0.6 ± 0.08 | 5.1 ± 0.28 | ⋆⋆ |

⋆ means anti-shadowing effects.

⋆⋆ means strong anti-shadowing effects.

This result agrees with macroscopic absorption cross sections data [26]. Enriched $B_4C$-90 has the highest macroscopic absorption cross sections followed by $Eu_2O_3$, $HfB_2$, $HfH_{1.62}$, and finally $Gd_2O_3$. The absorber materials are consumed during burnup. The effect of burnup on absorption ability will be investigated specifically in the second part of this paper.

Additionally, the worth of the CSD clusters is by factor 1.56 greater than the worth of the SSD system for all absorber materials. Both CSD and SSD clusters are separately able to shut down the reactor initially loaded by $^{233}U$ and reactor-grade Pu regardless of the absorber material type. However, only SSD clusters made of $B_4C$-90 is able to shut down the SD-TMSR initially loaded by transuranic (TRU) elements. Increasing the number of SSD cluster or changing their location would increase their worth.

The inner ring of the CSD is located in the central zone of the SD-TMSR core (Figure 4), where the ratio between molten salt and graphite moderator is 0.357. Results show that the inner ring of the CSD has the worth almost equal to the worth of all other CRs together regardless of the absorber material type (Table 2). This may be attributed to the fact that the absorption cross section decreases with the energy of incident neutron, for example, boron absorbs neutrons in thermal spectrum much greater than in fast spectrum.

In case of malfunction of the other CR clusters (e.g. stuck in the upper position), the outer ring of the CSD failures to counteract the excess reactivity of the core initially loaded by reactor-grade Pu and transuranic (TRU) elements. However, the worth of the outer ring of the CSD is sufficient to compensate the excess reactivity for the core with $^{233}U$ refueled.

We separately calculate the worth of CSD2, CSD9, SSD1, and SSD4 clusters to investigate the variation of CRW with the position in the active core. The CRW decreases in the direction of the peripheral zone. The peripheral zone has a high ratio between molten salt and graphite moderator about (1.162) compared with the central zone (0.357). As mentioned previously, the absorption ability decreases in fast spectrum.

Table 3: The shutdown margins for the SD-TMSR core for different absorber materials.

| Absorber materials | $^{233}U$ | reactor-grade Pu | TRU |
|---|---|---|---|
| $B_4C$-90 | $14.74 \pm 0.09$ \$ | $12.28 \pm 0.12$ \$ | $1.01 \pm 0.09$ \$ |
| $Eu_2O_3$ | $12.93 \pm 0.09$ \$ | $10.47 \pm 0.12$ \$ | $-0.8 \pm 0.09$ \$ |
| $HfB_2$ | $12.62 \pm 0.24$ \$ | $10.16 \pm 0.26$ \$ | $-1.11 \pm 0.24$ \$ |
| $HfH_{1.62}$ | $11.58 \pm 0.19$ \$ | $9.12 \pm 0.22$ \$ | $-2.15 \pm 0.19$ \$ |
| $Gd_2O_3$ | $10.35 \pm 0.22$ \$ | $7.89 \pm 0.25$ \$ | $-3.38 \pm 0.22$ \$ |

#### *4.2.2. Shutdown Margin (SDM)*

The SSD clusters are designed mainly for an emergency shutdown, thus it should provide the reactor core with sufficient and adequate negative reactivity. The shutdown margin (SDM) is calculated by equation 3. Table 3 summarizes the shutdown margins for the SD-TMSR core initially loaded by $^{233}$U, reactor-grade Pu, and transuranic (TRU) elements for different absorber materials. All absorber materials provide an adequate shutdown margin for the SD-TMSR core that initially loaded by $^{233}$U and reactor-grade Pu. However, the shutdown margins for TRU case are negative or slightly positive (in $B_4C$-90 case), this makes the SSD clusters ineffective to shut down the reactor in these cases.

#### *4.2.3. Interference between CR systems*

The amplification factor ($A_{CRi}$) results show that the CSD, SSD, CSD inner ring, and SSD1 are slightly amplified due to the anti-shadowing effects. The anti-shadowing is observed when the combined rod worth is greater than the sum of the individual worths. The strongest anti-shadowing effect has occurred in SSD4 and CSD9 clusters that are located at the boundary between the core zones with different moderator-to-fuel ratio (see Table 2). The obtained results emphasize the absence of the effect of the absorption material on the interference between the control rod clusters.

Insertion of the control rod affects the neutron flux distribution, which is the

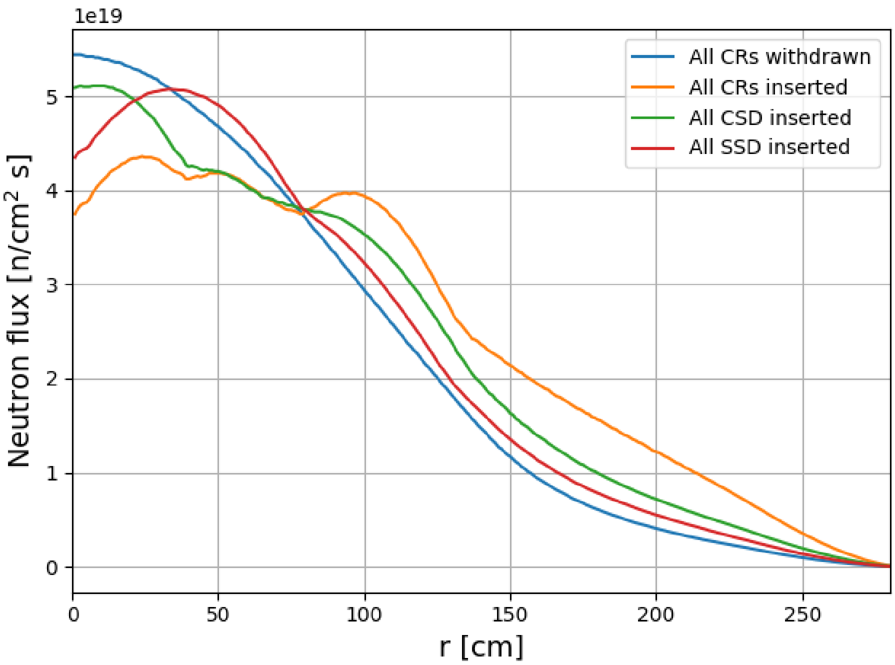


Figure 7: Radial neutron flux distribution at mid-core with different CRs position: (1) all CRs withdrawn (2) all CRs inserted (3) all CSD inserted (4) all SSD inserted.

basic reason for the amplification of CR worths indicated in Table 2. Figure 7 illustrates the radial neutron flux distribution at mid-core with different CRs position: (1) all CRs withdrawn (2) all CRs inserted (3) all CSD inserted (4) all SSD inserted. We chose the $B_4C$-90 as absorber materials because of its high absorption ability. As shown in Figure 7, the insertion of CRs deforms the radial flux shape in certain positions, i.e., around CRs positions. This shifts the neutron flux from the core center towards the periphery. A maximum neutron flux shift occurs when all CRs are inserted into the core.

#### *4.2.4. Integral and differential CRW*

The integral and differential control rod worth are calculated for three different systems: all control rods, CSD, and SSD systems. The CRs are inserted gradually into the core from top to bottom. Equation 5 and 6 are used to calculate the integral and differential CRW. Figure 8 illustrates the integral CRW for CRs made of $B_4C$-90. The maximum integral worth of All CRs, CSD, and SSD clusters are about 48.39 , 25.3, and 16.46 \$, respectively. The integral worth of SSD clusters is sufficient to shut down the reactor from any state.

The differential CRWs are demonstrated in Figure 9. Ideally, at the top of the core, the CR insertion has little effect since this region has low thermal neutron flux. Thus, the differential CRW has the lowest values in this region. The effect of CR insertion increases gradually near the center of the core. At the center of the core (region with maximum thermal neutron flux), the differential CRW is the largest and changes slowly with rod insertion. From the center of the core to the bottom, the differential CRW values decrease (region with low thermal neutron flux). Figure 9 shows that the maximum differential CRW is shifted toward the bottom of the core. This because (Need to find a reason(s)).

Figure 10 shows the integral CRW for only CSD clusters with five different absorber materials. The results show that all absorber materials have almost the same integral rod worth in the upper quarter of the core ($x$¡130). Further insertion of the control rod clusters shows the unique absorption characteristics of each material see part 4.2.1. Enriched $B_4C$-90 absorbs neutrons much grater than the $Gd_2O_3$ that has the lowest absorption ability among the other absorber materials in this study. All result are based on steady state calculations. Further and detailed analysis including burnup calculation will be represented in the near future.

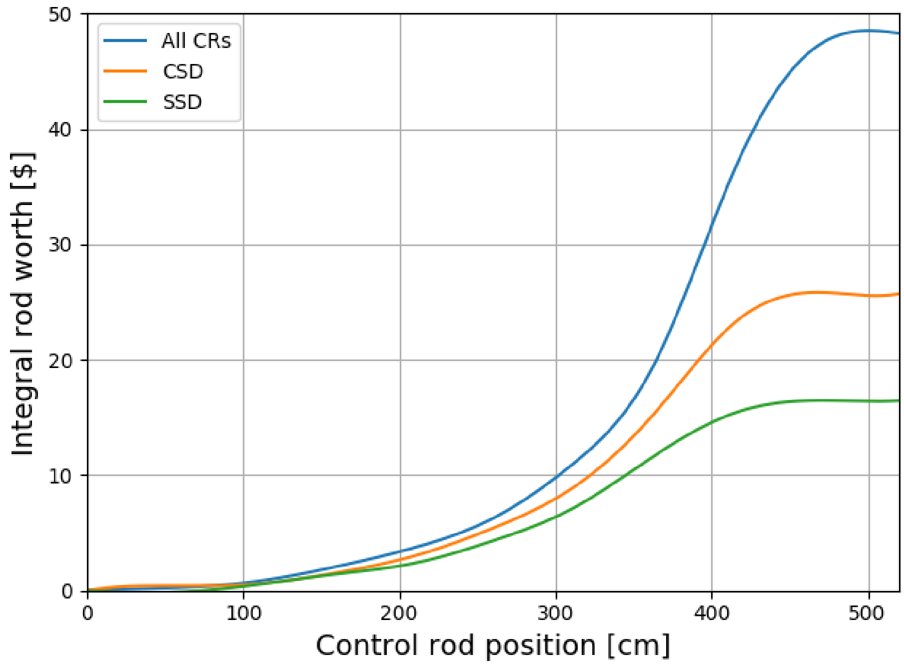

Figure 8: Integral control rod worth of all CRs, CSD, and SSD clusters.

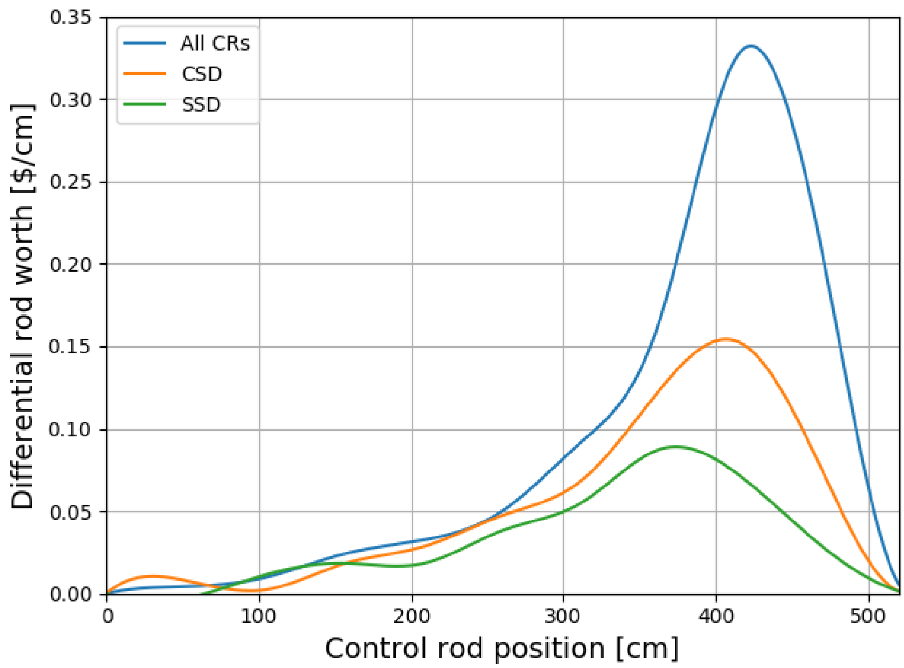

Figure 9: Differential control rod worth of all CRs, CSD, and SSD clusters.

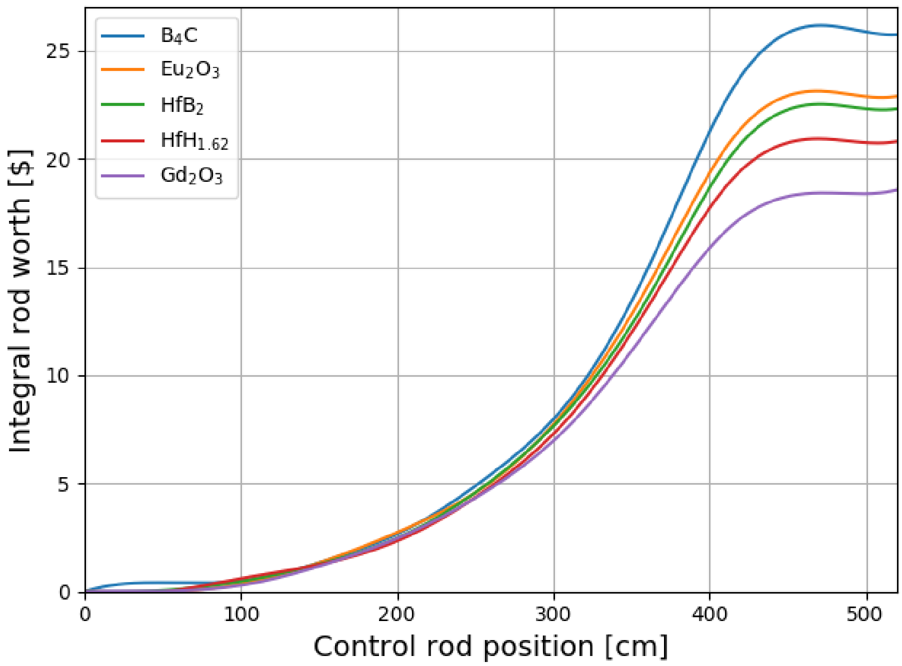


Figure 10: Integral control rod worth of CSD clusters for different absorber materials.

## 5. Conclusion

## 6. Future work

## 7. Declaration of Competing Interest

The authors declare that they have no known competing financial interests or personal relationships that could have appeared to influence the work reported in this paper.

## 8. Acknowledgments

Osama Ashraf would like to thank the Egyptian Ministry of Higher Education (MoHE), as well as MEPhI's Competitiveness Program for providing financial support for this research. The facility and tools needed to conduct this work were supported by MEPhI.

The authors contributed to this work as described below.

Osama Ashraf conceived and designed the simulations, wrote the paper, prepared figures and/or tables, performed the computation work, and reviewed drafts of the paper.

Andrei Rykhlevskii conceived and designed the simulations, wrote the paper, prepared figures and/or tables, performed the computation work, and reviewed drafts of the paper. Andrei Rykhlevskii is supported by DOE ARPA-E MEITNER program award DE-AR0000983.

G. V. Tikhomirov directed and supervised the work, conceived and designed the simulations and reviewed drafts of the paper. Prof. Tikhomirov is supported by Rosatom, he is Deputy Director of the Institute of Nuclear Physics and Engineering MEPhI. Board member of Nuclear society of Russia.

Kathryn D. Huff supervised the work, conceived and contributed to conception of the simulations, and reviewed drafts of the paper. Prof. Huff is supported by the Nuclear Regulatory Commission Faculty Development Program, the National Center for Supercomputing Applications, the NNSA Office of Defense Nuclear Nonproliferation R&D through the Consortium for Verification Technologies and the Consortium for Nonproliferation Enabling Capabilities, the International Institute for Carbon Neutral Energy Research (WPI-I2CNER), sponsored by the Japanese Ministry of Education, Culture, Sports, Science and Technology, and DOE ARPA-E MEITNER program award DE-AR0000983.

This research is part of the Blue Waters sustained-petascale computing project, which is supported by the National Science Foundation (awards OCI-0725070 and ACI-1238993) and the state of Illinois. Blue Waters is a joint effort of the University of Illinois at Urbana-Champaign and its National Center for Supercomputing Applications

## References

[1] DOE, US, A technology roadmap for generation iv nuclear energy systems (2002) 48–52.

[2] B. R. Betzler, A. Rykhlevskii, A. Worrall, K. Huff, Impacts of Fast-Spectrum

Molten Salt Reactor Characteristics on Fuel Cycle Performance, Tech. rep., Oak Ridge National Lab.(ORNL), Oak Ridge, TN (United States) (2019).

[3] O. Ashraf, A. Rykhlevskii, G. Tikhomirov, K. D. Huff, Whole core analysis of the single-fluid double-zone torium molten salt reactor (sd-tmsr), Annals of Nuclear Energy.
URL https://doi.org/10.1016/j.anucene.2019.107115

[4] B. R. Betzler, J. J. Powers, A. Worrall, Modeling and simulation of the start-up of a thorium-based molten salt reactor, in: Proc. Int. Conf. PHYSOR, 2016.

[5] M. H. Mohsin, K. Qureshi, T. Ashfaq, Safety assessment of msr concept using inpro methodology, Progress in Nuclear Energy 117 (2019) 103099.

[6] A. Zhang, C. Zou, J. Wu, S. Xia, C. Yu, J. Chen, Radiotoxicity of minor actinides in thermal, epithermal and fast tmsrs with very high burnup, Annals of Nuclear Energy 137 (2020) 107162.

[7] L. Mathieu, D. Heuer, R. Brissot, C. Garzenne, C. Le Brun, D. Lecarpentier, E. Liatard, J.-M. Loiseaux, O. Meplan, E. Merle-Lucotte, et al., The thorium molten salt reactor: Moving on from the msbr, Progress in Nuclear Energy 48 (7) (2006) 664–679.

[8] G. C. Li, P. Cong, C. G. Yu, Y. Zou, J. Y. Sun, J. G. Chen, H. J. Xu, Optimization of Th-U fuel breeding based on a single-fluid double-zone thorium molten salt reactor, Progress in Nuclear Energy 108 (2018) 144–151. doi:10.1016/j.pnucene.2018.04.017.
URL http://www.sciencedirect.com/science/article/pii/S0149197018300970

[9] B. M. Elsheikh, Safety assessment of molten salt reactors in comparison with light water reactors, journal of radiation research and applied sciences 6 (2) (2013) 63–70.

[10] E. Merle-Lucotte, D. Heuer, M. Allibert, X. Doligez, V. Ghetta, C. Le Brun, Optimization and simplification of the concept of non-moderated thorium molten salt reactor, in: International Conference on the Physics of Reactors-PHYSOR 2008, 2008.

[11] J. J. Duderstadt, L. J. Hamilton, Nuclear reactor analysis. 1976, Ann Arbor, Michigan: Wiley-Interscience 650.

[12] GLASSTONE-SESONSKE, Nuclear Reactor Engineering, Van Nostrand Reinhold C., 1967.

[13] M. Varvayanni, N. Catsaros, M. Antonopoulos-Domis, Estimation of irradiated control rod worth, Annals of Nuclear Energy 36 (11-12) (2009) 1706–1710.

[14] A. H. Fadaei, S. Setayeshi, Control rod worth calculation for vver-1000 nuclear reactor using wims and citation codes, Progress in Nuclear Energy 51 (1) (2009) 184–191.

[15] T. Aoyama, T. Sekine, S. Maeda, A. Yoshida, Y. Maeda, S. Suzuki, T. Takeda, Core performance tests for the joyo mk-iii upgrade, Nuclear Engineering and Design 237 (4) (2007) 353–368.

[16] M. Bretscher, Computing control rod worths in thermal research reactors, Argonne National Laboratory, Argonne, IllinoisFebruary 1997.

[17] G. Girardin, G. Rimpault, F. Morin, J. Bosq, P. Coddington, K. Mikityuk, R. Chawla, Development and characterization of the control assembly system for the large 2400 mwth generation iv gas-cooled fast reactor, Annals of Nuclear Energy 35 (12) (2008) 2206–2218.

[18] Š. Čerba, B. Vrban, J. Lüley, V. Nečas, J. Haščík, Optimization of the heterogeneous gfr 2400 control rod design, Progress in Nuclear Energy 97 (2017) 170–181.

[19] Y. Liu, R. Yan, Y. Zou, X. Kang, R. Ji, B. Zhou, S. Yu, Criticality properties and control rod worth of the critical experiment device for msr research, Nuclear Technology 204 (2) (2018) 203–212.

[20] S. Atkinson, D. Litskevich, B. Merk, Small modular high temperature reactor optimisation part 2: Reactivity control for prismatic core high temperature small modular reactor, including fixed burnable poisons, spectrum hardening and control rods, Progress in Nuclear Energy 111 (2019) 233–242.

[21] Q. B. Do, G. T. Phan, K.-C. Nguyen, Q. H. Ngo, H.-N. Tran, Criticality and rod worth analysis of the dnrr research reactor using the srac and mcnp5 codes, Nuclear Engineering and Design 343 (2019) 197–209.

[22] H. Guo, P. Archier, J.-F. Vidal, L. Buiron, Advanced method for depletion calculation of control rods in sodium fast reactors, Annals of Nuclear Energy 129 (2019) 160–168.

[23] Z. Zhong, A. Abou-Jaoude, F. Heidet, Preliminary control rod lifetime assessment for the versatile test reactor, in: Transactions of the 2019 ANS Annual Meeting, American Nuclear Society, 2019.

[24] M. Steinbrück, Degradation and oxidation of b4c control rod segments at high temperatures, Journal of Nuclear Materials 400 (2) (2010) 138–150.

[25] P. Dünner, H.-J. Heuvel, M. Hörle, Absorber materials for control rod systems of fast breeder reactors, Journal of nuclear materials 124 (1984) 185–194.

[26] H. Guo, L. Buiron, T. Kooyman, P. Sciora, Optimized control rod designs for generation-iv fast reactors using alternative absorbers and moderators, Annals of Nuclear Energy 132 (2019) 713–722.

[27] D. Gosset, Absorber materials for generation iv reactors, in: Structural Materials for Generation IV Nuclear Reactors, Elsevier, 2017, pp. 533–567.

[28] R. Konings, Comprehensive nuclear materials, Elsevier, 2011.

[29] A. Rykhlevskii, J. W. Bae, K. D. Huff, Modeling and simulation of online reprocessing in the thorium-fueled molten salt breeder reactor, Annals of Nuclear Energy 128 (2019) 366–379. doi:10.1016/j.anucene.2019.01.030.

[30] O. Ashraf, A. Smirnov, G. Tikhomirov, Nuclear fuel optimization for molten salt fast reactor, in: Journal of Physics: Conference Series, Vol. 1133, IOP Publishing, 2018, p. 012026. doi:doi:10.1088/1742-6596/1133/1/012026.

[31] O. Ashraf, A. Smirnov, G. Tikhomirov, Modeling and criticality calculation of the molten salt fast reactor using serpent code, in: Journal of Physics: Conference Series, Vol. 1189, IOP Publishing, 2019, p. 012007.

[32] G. Girardin, G. Rimpault, P. Coddington, R. Chawla, Control rod shadowing and antishadowing effects in a large gas-cooled fast reactor, in: Proceedings of ICAPP, Vol. 7, 2007, pp. 13–18.

[33] J. F. Briesmeister, et al., Mcnptm-a general monte carlo n-particle transport code, Version 4C, LA-13709-M, Los Alamos National Laboratory (2000) 2.

[34] L. M. Petrie, N. F. Landers, Keno va: an improved monte carlo criticality program with supergrouping, Tech. rep. (1984).

[35] J. Leppänen, M. Pusa, T. Viitanen, V. Valtavirta, T. Kaltiaisenaho, The serpent monte carlo code: Status, development and applications in 2013, in: SNA+ MC 2013-Joint International Conference on Supercomputing in Nuclear Applications+ Monte Carlo, EDP Sciences, 2014, p. 06021.

[36] M. Jiang, H. Xu, Z. Dai, Advanced fission energy program-tmsr nuclear energy system, Bull. Chin. Acad. Sci 27 (3) (2012) 366–374.

[37] X. Li, X. Cai, D. Jiang, Y. Ma, J. Huang, C. Zou, C. Yu, J. Han, J. Chen, Analysis of thorium and uranium based nuclear fuel options in fluoride salt-cooled high-temperature reactor, Progress in Nuclear Energy 78 (2015) 285–290.

[38] G. Li, Y. Zou, C. Yu, et al., Model optimization and analysis of th–u breeding based on msfr, Nucl. Tech 40 (2017) 020603–020603.

[39] R. C. Robertson, Conceptual Design Study of a Single-Fluid Molten-Salt Breeder Reactor., Tech. Rep. ORNL–4541, comp.; Oak Ridge National Laboratory, Tenn. (Jan. 1971).
URL http://www.osti.gov/scitech/biblio/4030941

[40] A. Nuttin, D. Heuer, A. Billebaud, R. Brissot, C. Le Brun, E. Liatard, J.-M. Loiseaux, L. Mathieu, O. Meplan, E. Merle-Lucotte, et al., Potential of thorium molten salt reactorsdetailed calculations and concept evolution with a view to large scale energy production, Progress in nuclear energy 46 (1) (2005) 77–99.

[41] J. C. Marka, Explosive properties of reactor-grade plutonium, Science & Global Security 4 (1) (1993) 111–128.

[42] C. de Saint Jean, M. Delpech, J. Tommasi, G. Youinou, P. Bourdot, Scénarios cne: réacteurs classiques, caractérisation à l'équilibre, rapport CEA DER/SPRC/LEDC/99-448.

[43] J.-L. Sran, M. L. Flem, 8 - irradiation-resistant austenitic steels as core materials for generation iv nuclear reactors, in: P. Yvon (Ed.), Structural Materials for Generation IV Nuclear Reactors, Woodhead Publishing, 2017, pp. 285 – 328. doi:https://doi.org/10.1016/B978-0-08-100906-2.00008-2.
URL http://www.sciencedirect.com/science/article/pii/B9780081009062000082

[44] J. Leppänen, M. Aufiero, E. Fridman, R. Rachamin, S. van der Marck, Calculation of effective point kinetics parameters in the serpent 2 monte carlo code, Annals of Nuclear Energy 65 (2014) 272–279.

[45] V. Ignatiev, O. Feynberg, A. Merzlyakov, A. Surenkov, A. Zagnitko, V. Afonichkin, A. Bovet, V. Khokhlov, V. Subbotin, R. Fazilov, et al.,

Progress in development of mosart concept with th support, in: Proceedings of ICAPP, Vol. 12394, 2012.

[46] D. Sood, P. Iyer, R. Prasad, V. Vaidya, K. Roy, V. Venugopal, Z. Singh, M. Ramaniah, Plutonium trifluoride as a fuel for molten salt reactors-solubility studies, Nuclear technology 27 (3) (1975) 411–415.

[47] C. Zou, C. Cai, C. Yu, J. Wu, J. Chen, Transition to thorium fuel cycle for tmsr, Nuclear Engineering and Design 330 (2018) 420–428.

[48] A. Rykhlevskii, A. Lindsay, K. D. Huff, Full-core analysis of thorium-fueled Molten Salt Breeder Reactor using the SERPENT 2 Monte Carlo code, in: Transactions of the American Nuclear Society, American Nuclear Society, Washington, DC, United States, 2017.

[49] B. Forget, K. Smith, S. Kumar, M. Rathbun, J. Liang, Integral Full Core Multi-Physics PWR Benchmark with Measured Data, Tech. rep., Massachusetts Institute of Technology (2018).

[50] N. G. Sjöstrand, J. S. Story, Cross sections and neutron yields for U-233, U-235 and Pu-239 at 2200 m/sec, Tech. rep., AB Atomenergi (1960).

[51] J. Park, Y. Jeong, H. C. Lee, D. Lee, Whole core analysis of molten salt breeder reactor with online fuel reprocessing, International Journal of Energy Research 39 (12) (2015) 1673–1680. `doi:10.1002/er.3371`.
URL `http://doi.wiley.com/10.1002/er.3371`

[52] A. Rykhlevskii, J. W. Bae, K. Huff, arfc/saltproc: Code for online reprocessing simulation of molten salt reactor with external depletion solver SERPENT, Zenodo`doi:10.5281/zenodo.1196455`.
URL `https://zenodo.org/record/1196455#.WqrE_BPwaA0`

[53] A. Rykhlevskii, K. Huff, Milestone 2.1 Report: Demonstration of SaltProc, Milestone Report UIUC-ARFC-2019-04 DOI: 10.5281/zenodo.3355649, University of Illinois at Urbana-Champaign, Urbana, IL (Jun. 2019).

doi:10.5281/zenodo.3355649.
URL https://zenodo.org/record/3355649#.XZuyEEFKjdI

[54] A. Lindsay, G. Ridley, A. Rykhlevskii, K. Huff, Introduction to Moltres: An application for simulation of Molten Salt Reactors, Annals of Nuclear Energy 114 (2018) 530–540. doi:10.1016/j.anucene.2017.12.025.